



# Performance of the Medipix and Timepix devices for the recognition of electron-gamma radiation fields <sup>☆</sup>

C. Teyssier <sup>a,c,d,\*</sup>, J. Bouchami <sup>a</sup>, F. Dallaire <sup>a</sup>, J. Idárraga <sup>a</sup>, C. Leroy <sup>a</sup>, S. Pospíšil <sup>b</sup>, J. Solc <sup>b</sup>,  
O. Scallan <sup>a</sup>, Z. Vykydal <sup>b</sup>

<sup>a</sup> Université de Montréal, Montréal (Québec) H3C 3J7, Canada

<sup>b</sup> Czech Technical University in Prague, Institute of Experimental and Applied Physics, Horska 3a/22, CZ-128 00 Praha 2, Czech Republic

<sup>c</sup> Université de Lyon, F-69003, Lyon, France – Université Claude Bernard Lyon 1, Villeurbanne, France

<sup>d</sup> CNRS/IN2P3, UMR5822, Institut de Physique Nucléaire de Lyon, F-69622 Villeurbanne, France

## ARTICLE INFO

Available online 21 December 2010

### Keywords:

Medipix  
Mistagging  
Compton  
Detection efficiency  
Timepix

## ABSTRACT

The Medipix device is a silicon pixelated detector designed by CERN for the detection of different types of radiation. The detector response features can be exploited to identify different types of particles: heavy charged particles, mips, electrons or photons. However, while heavily ionizing charged particles are clearly recognizable, electrons and photons can hardly be distinguished from each other and thus, mistagging of radiation quanta has to be considered. Experiments were performed to quantify the mistag rate in different experimental situations. A GEANT4 simulation of the detector and the experimental setup was used to further understand the results. The detection efficiency for photons was studied and the advantages of using a Timepix device highlighted.

© 2010 Elsevier B.V. All rights reserved.

## 1. Introduction

The Medipix device [1] is composed of a 300  $\mu\text{m}$  thick silicon layer bonded to a pixelated read-out chip. The cathode has  $256 \times 256$  pixels, each of  $55 \times 55 \mu\text{m}^2$  area. When hitting the silicon layer, the particles deposit energy by creating electron–hole pairs. Because of the charge sharing effect [2], the charge carriers are spread before being collected. The signal induced in each pixel is compared to a preset threshold. If the signal is larger than a preset threshold, the pixel is activated. A particle can activate one or several pixels forming a blob. The data are recorded as frames that contains the status of all the pixels (65 536) after a given acquisition time.

A pattern recognition algorithm developed in the context of the Medipix Analysis Framework MAFalda [3] uses the blob shape to recognize the different types of blobs which can be associated to a specific type of particle. These associations are efficient for heavy particles recognition. However, because of the mechanism of detection, mis-associations may occur when identifying photons and electrons. Therefore, experiments were necessary to evaluate the number of occurrences of mis-associations in different

experimental configurations. These experiments are presented in Section 2. As photons cannot be identified or their flux properly estimated, the electrons produced by photons in air and surrounding materials have a role in the detection efficiency and their influence is studied in Section 3. In that study, a Timepix detector was used and results were compared with a GEANT4 simulation implemented by the authors. The Timepix device [4] has the same structure as the Medipix device. However it is equipped with a clock that allows the measurement of the time during which the signal is over threshold in each pixel. Thus the energy deposit in each pixel can be evaluated after calibration.

## 2. Mistagging







MAFalda permits the analysis of the frames and the classification of the different types of blobs by their shape. In Fig. 1, the names of each type are listed in the left column and it can be associated to a particle (right column of Fig. 1). These associations are valid under certain experimental conditions, such as the value of the preset energy threshold [5].

Heavy charged particles like protons or alpha-particles will deposit energy via Coulomb interaction and activate several pixels. Their tracks will typically appear as heavy blobs or heavy tracks depending on their energy and incidence (Fig. 1). Mips leave very long straight tracks easily recognizable except when they hit perpendicularly the silicon layer and thus activate only a few pixels.

<sup>☆</sup> This work was carried out within the CERN Medipix Collaboration.

\* Corresponding author at: Université Claude Bernard Lyon 1, Institut de Physique Nucléaire de Lyon, Groupe Interactions Particules Matière, Bâtiment Paul Dirac, 4 rue Enrico Fermi, 69622 Villeurbanne, France.

E-mail addresses: c.teyssier@ipnl.in2p3.fr, teyssier@lps.umontreal.ca (C. Teyssier).

Single, double, triple, quadruple hits		Photons and electrons
Long Gamma		Photons and electrons
Heavy blobs		Heavy ionizing particles
Heavy tracks		Heavy ionizing particles → Incidence is not perpendicular to the detector's surface (Bragg curve)
Straight tracks		MIP
Curly tracks		Energetic electrons

**Fig. 1.** Examples of blob shapes generated by different types of particles in the Medipix device. The association is valid under certain experimental conditions (see text).

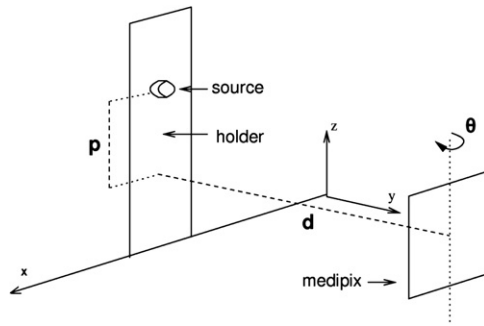


**Fig. 2.** Experimental setup.  $d$  is the distance between the holder and the detector and  $p$  the height of the source on the holder with respect to the center of the detector.  $\theta$  is the rotation angle of the detector with respect to the  $z$ -axis.

Light particles such as electrons interact also by Coulomb interaction but due to their small mass, they have random trajectories. Depending on their energy, they will appear as single, double, triple and quadruple hits, long gamma and curly tracks (Fig. 1). Photons are detected indirectly. They can deposit energy through three interactions: photoelectric effect, Compton scattering and pair creation. In each case, they transfer all or part of their energy to light charged particles, i.e., electrons or/and positrons, which are detected. Therefore, it is a priori not possible to distinguish electrons from photons. Knowing the experimental context (energy and intensity of photons and electrons), one can make a choice of configuration (each blob type is associated with a particle type). Usually, due to the 100% detection efficiency of the Medipix detector for the electrons, curly tracks are related to electrons rather than to Compton electrons produced by an energetic photon. When identification is required to calculate observables such as the activity of a source, mis-association becomes a major obstacle and has to be evaluated. Then, the question arises: When a particle is identified as a photon, what is the probability that it is in fact an electron? To answer this question, experiments were carried out at the Université de Montréal to measure the rate of mistagging.

The experimental setup is shown in Fig. 2. The purpose is to study a mixed field of photons and electrons produced by a  $^{106}\text{Ru}$  and a  $^{137}\text{Cs}$  source. The sources are mounted on a holder at a distance  $d$  from the detector which can be rotated clockwise with respect to the  $z$ -axis. The experiments are performed in a vacuum of  $2 \times 10^{-6}$  Torr. The characteristics of the sources can be found in Table 1. The fraction  $F_\theta$  of solid angle of the detector is calculated for each angle (the source dimensions are taken into account). The

**Table 1**

Characteristics of the sources used in the experimental setup. The  $p$  and  $d$  distances are depicted in Fig. 2.

Source	Activity (kBq)	$\gamma$ , X-ray emission fraction	$e^-$ , $\beta$ emission fraction	$p, d$ (mm)
$^{106}\text{Ru}$	76.59	1.002	1.000	14.3, 67.7
$^{137}\text{Cs}$	81.15	0.035	1.197	25.4, 67.7

threshold of the Medipix is set at 7.8 keV and the depletion voltage at 100 V.

The activity is reconstructed in three different cases: firstly all the tracks are considered ( $R_{all}$  rate), secondly only those associated with electrons ( $R_{e^-}$  rate) and thirdly only those associated with photons and X-rays ( $R_{\gamma,X}$  rate). The following formula (1)–(3) are used.

$$A_{s_1} = \frac{R_{all}}{F_\theta \times (f_{\gamma,X} + f_{e^-})} \quad (1)$$

$$f_{\gamma,X} = \sum_{i=\gamma,X} I_i \times \eta_i, \quad f_{e^-} = \sum_{i=e^-} I_i \quad (2)$$

$$A_{s_2} = \frac{R_{e^-}}{F_\theta \times f_{e^-}}, \quad A_{s_3} = \frac{R_{\gamma,X}}{F_\theta \times f_{\gamma,X}} \quad (3)$$

where  $A_{s_1}$ ,  $A_{s_2}$ ,  $A_{s_3}$  are the activity of the source calculated in the first, second and third case,  $I_i$  is the intensity of particles  $i$  whose energy is above threshold for the given source,  $\eta_i$  is the detection efficiency for particles  $i$ . For electrons, the detection efficiency is 100% and the factor  $f_{e^-}$  is just the emission intensity.

In Fig. 3(a), the reconstructed activity for the  $^{106}\text{Ru}$  source is shown for several angles between  $0^\circ$  and  $90^\circ$ . The set of points marked as combined corresponds to the first case where all the tracks are considered (Eq. (1)). The activity of the source known within  $\pm 5\%$  precision is represented by the parallel lines around 76.59 kBq. For every angle, the reconstruction is successful. In the same figure, the other cases are shown. For this purpose, the blobs are separated in two types: photons and electrons. Then, the activity is calculated with Eqs. (3). The difficult part is to determine which traces arise from photons and which ones from electrons. Several configurations are distinguished and the corresponding reconstructions are shown in Figs. 3(a)–(e). In the first configuration, single, double, triple, quadruple and long gamma blobs are considered as photons and curly as electrons. At  $0^\circ$ , the activity is clearly over-reconstructed for photons and under-reconstructed for electrons which means that some electrons are wrongly tagged as photons. The situation is reversed at  $75^\circ$ . The activity is very well reconstructed in both cases at  $45^\circ$  and  $90^\circ$  but it does not mean that the particles are properly tagged for these particular angles. A good reconstruction can be apparently achieved if the same amount of photons and electrons has been mis-associated, cancelling the mistagging effect.

The other configurations are explored by switching the blobs types from photon type to electron type until only the single hits are considered as photons. The evolution of the configuration is shown in Figs. 3(b)–(e). In Fig. 3(b), associating long gamma to electrons instead of photons improves reconstruction at  $0^\circ$ . For larger angle, the reconstruction is over-estimated for electrons and under-estimated for photons. It means that the Compton or photoelectric electrons produced by photons at higher angle have a longer path in the silicon layer and thus give larger blobs. This tendency is amplified for the next configurations. None of the configuration provides satisfying results for all angles. The reason is that photons produce small and long tracks (the energy transferred to Compton electrons varies and the location of the electrons created in the silicon layer has consequences on the charge sharing

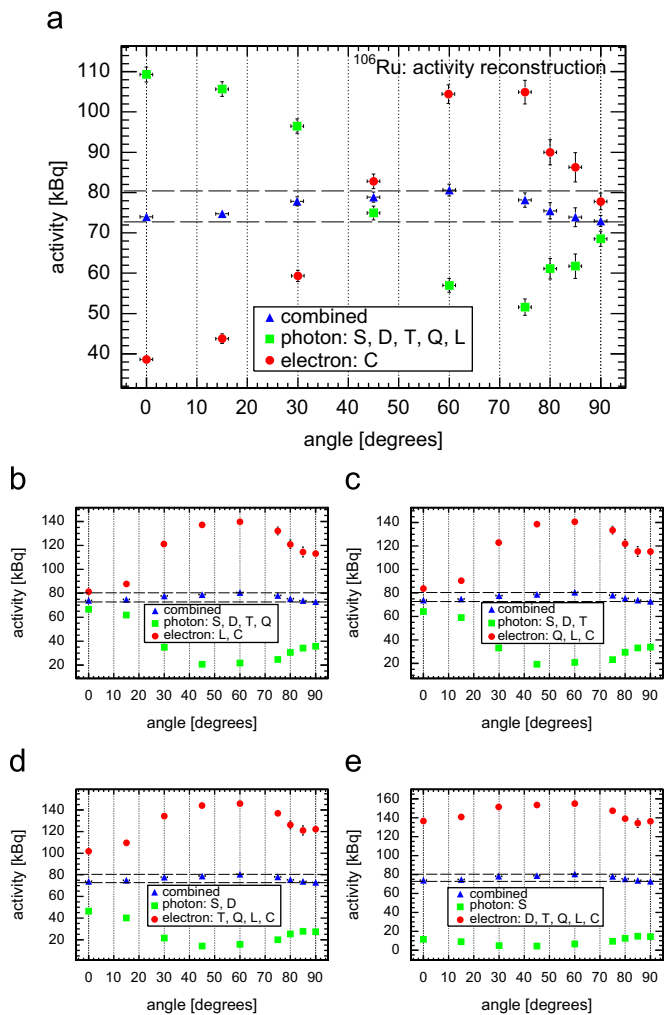


**Fig. 3.**  $^{106}\text{Ru}$  activity reconstruction in different configurations. The different blob types: single (S), double (D), triple (T), quadruple (Q), long gamma (L), curly (C) are associated to photons or electrons. (a) Configuration 1. Only curly tracks are associated to electron. (b) Configuration 2. Long gamma type switched from photon type to electron type. (c) Configuration 3. Quadruple hits switched from photon type to electron type. (d) Configuration 4. Triple hits switched from photon type to electron type. (e) Configuration 5. Double hits switched from photon type to electron type.

effect). The mis-association is inherent to the detection technique and so unavoidable.

A similar study was undertaken with a source of  $^{137}\text{Cs}$ . Results are presented in Fig. 4. The reconstruction of activity is accurate when no particle identification is performed. The mis-association for photons happens more often than in the case of  $^{106}\text{Ru}$  as the photon energy is higher. Therefore, the probability of interaction in silicon is lower and the energy of Compton electrons higher. The most relevant photon emission from  $^{137}\text{Cs}$  is around 662 keV. The corresponding Compton electrons have a mean energy of 253 keV with a maximum energy of 478 keV. Photons can then produce long tracks. Through the evolution of configuration, there is an improvement in the reconstruction for electrons. It is even better to consider all the blobs as electrons (Fig. 5) because of the low probability of interaction of photons (compared to that of electrons).

At this energy of 662 keV, it is very difficult to reconstruct the activity from photons. At larger angles, the reconstruction improves because the effective thickness of the silicon layer is larger and the detection efficiency is improved. But the reconstruction with photons is off by excess for every case. The limits of the association blobs-to-

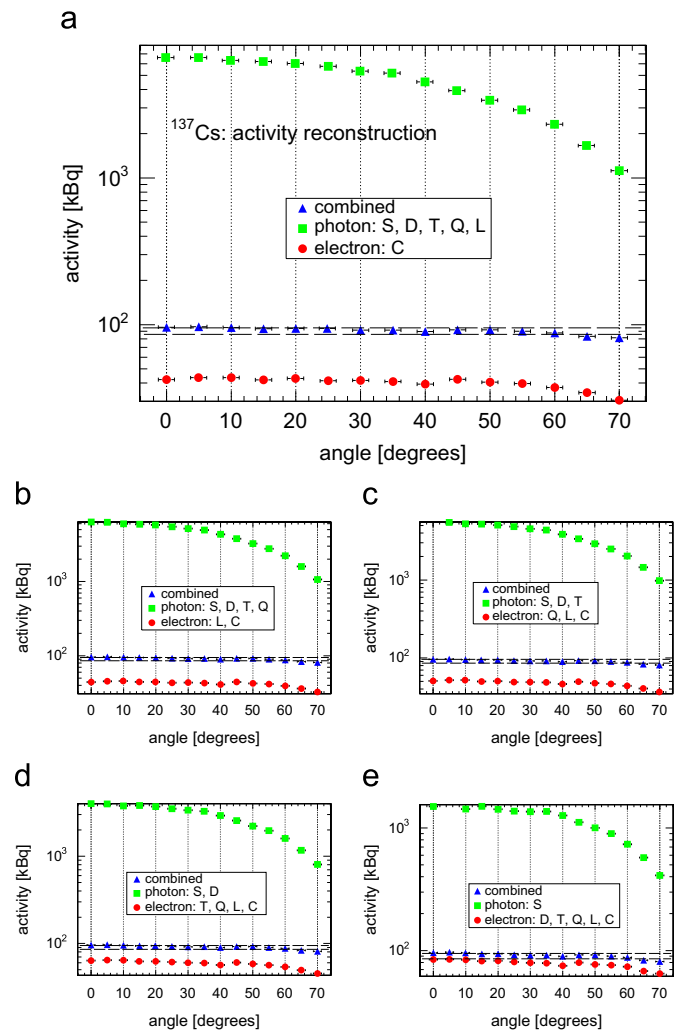


**Fig. 4.**  $^{137}\text{Cs}$  activity reconstruction in different configurations. The different blob types: single (S), double (D), triple (T), quadruple (Q), long gamma (L), curly (C) are associated to photons or electrons. (a) Configuration 1. Only curly tracks are associated to electron. (b) Configuration 2. Long gamma type switched from photon type to electron type. (c) Configuration 3. Quadruple hits switched from photon type to electron type. (d) Configuration 4. Triple hits switched from photon type to electron type. (e) Configuration 5. Double hits switched from photon type to electron type.

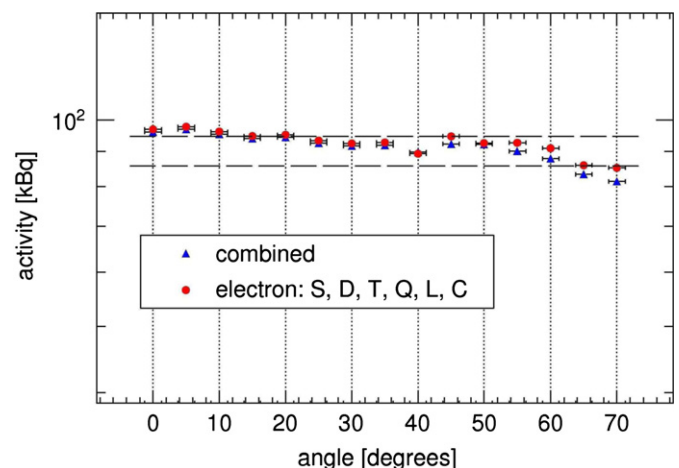


**Fig. 5.** Configuration 6: all types are considered as electrons.

particles are reached here and no better association can be done with a Medipix2 device under the conditions presented here.

The conclusion of these studies is that mis-association strongly depends on several aspects, namely: the energy and incident angle of the particles hitting the silicon layer and the configuration setup. It is therefore not straightforward to extrapolate the rate of mistagging to another mixed field of radiations.

### 3. Study of Compton effect

A network of Medipix devices (ATLAS-MPX) is operating at LHC to measure the composition of the radiation field within the ATLAS detector [6]. Due to their 100% detection efficiency for charged particles (at low threshold), the ATLAS-MPX devices are much more sensitive to electrons than gamma rays for which the detector efficiency falls under 1% for energy higher than 270 keV. For photons of 1 GeV and above, the detector efficiency is quasi-constant, with a value of 0.25%. The ATLAS-MPX detectors are surrounded by air and different materials where photons can produce electrons which can reach the detector and be detected. This will somehow change the detector efficiency for photons. The following experiment aims at the evaluation of these changes.

Experiments were carried out with the  $^{137}\text{Cs}$  source used in Section 2 for which a simplified spectrum is given in Table 2. The same experimental setup (Fig. 2) is used except that this time, experiments will be done in the air and in the vacuum and the incident angle is always  $0^\circ$  (i.e., the plane of the sensor is parallel to the plane of the holder of the sources). A layer of aluminium is placed in front of the source to eliminate the electrons emitted by the source. The Medipix detector is replaced with a Timepix detector. The thickness of the aluminium layer, 3.07 mm, was chosen to be large enough to stop all the electrons from the source (the highest energy of  $^{137}\text{Cs}$  electrons is 1.175 MeV which corresponds to a maximal range in aluminium of 2.5 mm). It is noteworthy that the introduction of such a layer produces another source of photoelectric and Compton electrons. Then, electrons can be created in the air, in the layer of aluminium and in other materials surrounding the detector. The theoretical detection probability of photons from the  $^{137}\text{Cs}$  source was calculated with Eq. (4) without considering the detection of photon-produced electrons (right column of Table 2):

$$\eta_i = \prod_{j=\text{Al,air}} e^{-(\mu/\rho)_{j,i} \rho_j x_j} \times (1 - e^{-(\mu/\rho)_{\text{Si},i} \rho_{\text{Si}} x_{\text{Si}}}) \quad (4)$$

where  $\eta_i$  is the detector detection efficiency for the photons  $i$ ,  $\mu/\rho_{j,i}$  the mass absorption coefficient of photons  $i$  in material  $j$ ,  $\rho_j$  and  $x_j$  the volumic mass and effective thickness of material  $j$ , respectively.

Then, the rate of detected photons given by Eq. (5) is found to be  $1.64 \pm 0.10$  per second both in air and in vacuum (the attenuation in air is negligible).

$$\text{flux} = A_s \times F_\theta \times \sum_{i=\gamma,X} I_i \times \eta_i \quad (5)$$

(same notations as in Eqs. (1)–(3))

**Table 2**

Simplified gamma spectrum of  $^{137}\text{Cs}$  [7], only the emissions with energy above the detector threshold (7.8 keV) are considered. The probability of gamma detection is calculated for each energy using Eq. (4).

Energy of gamma (keV)	Emission fraction	Theoretical probability of gamma detection $\eta_i$ (%)
32	$5.8 \times 10^{-2}$	3.69
36	$1.3 \times 10^{-2}$	3.42
662	$85.2 \times 10^{-2}$	0.53

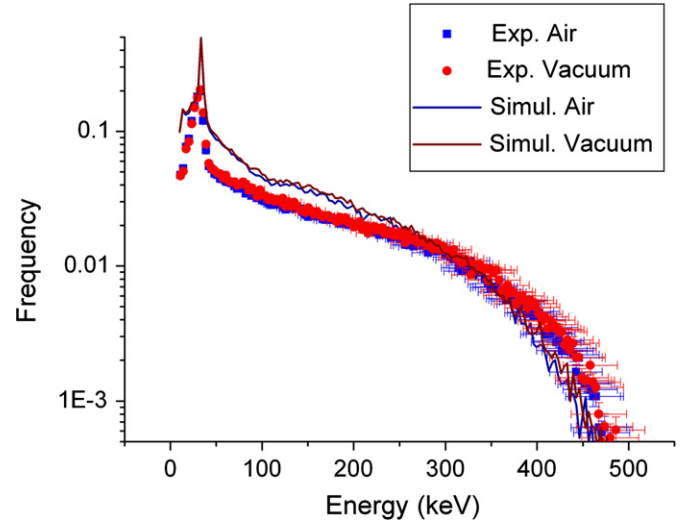


**Fig. 6.** Experimental and simulated energy spectra of all hits in air and in vacuum.

The experiments were performed with an energy threshold of 7.8 keV and an acquisition time of 6 s. The total measured rate is  $3.75 \pm 0.06 \text{ s}^{-1}$  in air and  $3.89 \pm 0.07 \text{ s}^{-1}$  in vacuum. The ratio air/vacuum is  $0.964 \pm 0.033$ . These rates are much higher than the theoretical rate (calculated above) because the secondary sources (Al-filter, surrounding materials) are not taken into account in the calculation.

As a Timepix detector was used, the time over threshold of all activated pixels were recorded. Thanks to a previous calibration (see Ref. [8] for the calibration method), the distribution in energy of the detected events is obtained and displayed in Fig. 6. In this normalized distribution, there is a peak around 35 keV corresponding to the detection of photons of 32 and 36 keV that produce electrons by photoelectric effect mostly. The rest of the spectrum is associated to the 662 keV photons that interact mostly via Compton scattering [9]. It is compatible with the maximal energy of 478 keV of Compton electrons produced by 662 keV photons. These Compton electrons have a mean energy of 253 keV. Those produced in silicon can get out the sensitive layer and thus, do not deposit all their energy. The electrons produced in air or in surrounding materials can lose various amounts of energy before reaching the detector (depending on their paths). That is supported by the absence of peak around 253 keV.

A simulation of the experiment was done with GEANT4 [10,11] to understand the origin of the differences between theoretical and experimental rates. In Fig. 7, an image of the structures used is displayed: the cylindrical chamber, the holder of the source, the holder of the detector, the USB interface, the aluminium layer, the source and the detector on its PCB support. The Timepix behaviour is reproduced and 5000 frames for each experiment (air and vacuum) were generated.

The simulated and experimental spectra have the same structure allowing the validation of the simulation (see Fig. 6). The simulated rates in air and in vacuum were found to be  $4.97 \pm 0.07$  and  $5.12 \pm 0.08 \text{ s}^{-1}$ , respectively. These values are higher than the measured values. One can see in Fig. 6 that in the simulation, the low energy event rate is over-estimated and the high energy event rate slightly under-estimated. This is due to a rough geometry description of the surroundings of the detector and the vacuum chamber. In this case, the limits of the chamber are very close to the sensor and irregularities introduced by the experiment services all around (cables, screws, etc.) become important. Thus, an extremely precise geometry description of the surroundings is mandatory to simulate properly the transport and particle conversion in GEANT4



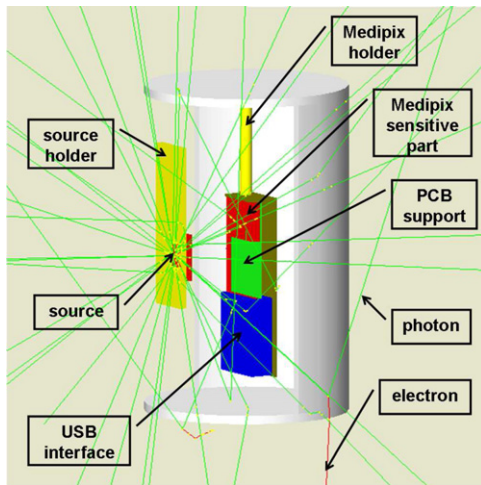


Fig. 7. Simulation of the experiments with GEANT4.

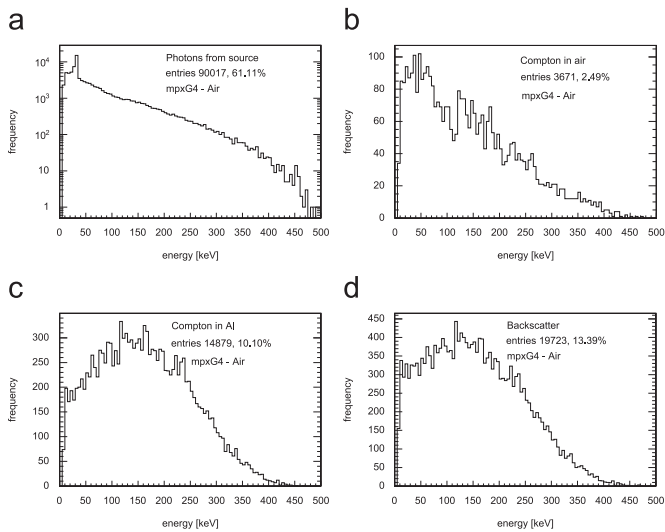


Fig. 8. Energy spectra and percentages of detected particles depending on their origin. (a) Photons coming directly from the source. (b) Electrons created in air. (c) Electrons created in the aluminium layer. (d) Electrons created everywhere else (backscattered).

and to reproduce exact results. At this point, what we obtain in Fig. 6 reproduces properly the overall behaviour and validates our digitalization of a Medipix2 device in GEANT4 implementation which is enough to understand the lack of separation-power between experiments done in vacuum and air. The ratio between air and vacuum is  $0.970 \pm 0.029$  in the simulation which is very close to the experimental ratio. The simulation in GEANT4 allows us to find where the Compton or photoelectric electrons are produced before being detected. In Fig. 8(a)–(d), the spectra and corresponding percentage of electrons from air, aluminium, chamber and holders in the experiment in air are shown. The proportion of photons coming directly from the source in the simulation is  $61.1 \pm 2.3\%$  and  $58.7 \pm 2.5\%$  in air and vacuum, respectively. These values are higher than the value of  $43.7 \pm 3.3\%$  for air and  $42.2 \pm 3.2\%$  for vacuum obtained in the experiments. The simulation gives promising results and should be improved by a better definition of experimental elements. The detection efficiency for photons from  $^{137}\text{Cs}$  in this experimental setup can be corrected by a factor  $f_{\text{air}} = 2.29 \pm 0.18$  and  $f_{\text{vacuum}} = 2.37 \pm 0.19$ . It appears that the events originating from air are less important than the events

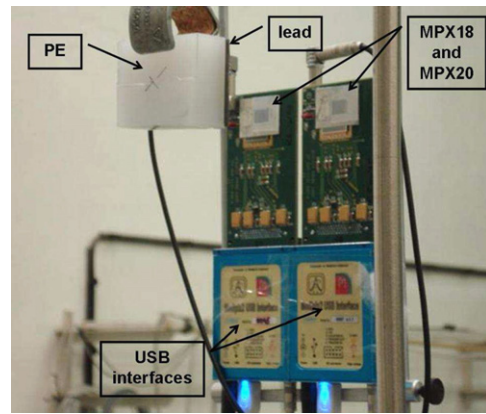


Fig. 9. Experimental setup at CMI. A layer of PE (2 cm thick) and a layer of lead (500  $\mu\text{m}$  thick) permit the study of the detectors response to photons.

Table 3

Results of CMI experiments for the  $^{252}\text{Cf}$  and the  $^{241}\text{AmBe}$  source. The ratio of measured flow over theoretical flow is shown in the last column for both detectors and sources.

Medipix	Measured flow ( $\text{s}^{-1}$ )	Theoretical flow ( $\text{s}^{-1}$ )	Ratio
$^{252}\text{Cf}$ source, 914 keV photons			
MPX18	$263.52 \pm 0.93$	$50.24 \pm 1.30$	$5.24 \pm 0.15$
MPX20	$166.14 \pm 0.91$	$32.51 \pm 0.84$	$5.11 \pm 0.16$
$^{241}\text{AmBe}$ source, 4.438 MeV photons			
MPX18	$32.81 \pm 0.07$	$3.57 \pm 0.09$	$9.19 \pm 0.25$
MPX20	$20.03 \pm 0.05$	$2.31 \pm 0.06$	$8.67 \pm 0.24$

originating from surrounding materials. In the real ATLAS MPX experiment, the Medipix are surrounded by diverse materials (Medipix holder and services of the ATLAS detector). If one want to use tracks from light particles (for dosimetry for example), all those materials have to be taken into account to find the correct fluxes.

Other experiments were done at the Czech Metrological Institute (CMI) in Prague with two Medipix detectors (MPX18 and MPX20) exposed to a  $^{252}\text{Cf}$  and a  $^{241}\text{AmBe}$  source. In order to get rid of neutrons, a layer of polyethylene (PE) was placed in front of the sources. A thin layer of lead stopped the recoiled protons produced by neutrons in PE (Fig. 9).

In Table 3, theoretical and measured flows are compared. The correction factor is evaluated to be  $5.18 \pm 0.11$  and  $8.93 \pm 0.18$  for 914 keV and 4.438 MeV photons, respectively.

These experiments show that the correction factor depends on the energy of photons. Then, the knowledge of the energy of photons is necessary to analyse the recorded data. This information can be provided to a certain extent by a Timepix detector as can be seen in Fig. 6.

#### 4. Conclusion

Two studies were presented in this work. The first addresses the question of the identification of light particles in a mixed field. It has been shown that the mistag rate in particle selection can be evaluated under the present experimental conditions but it is not straightforward to extrapolate the results to other mixed radiation fields. We prove the key point of association blob-to-particle to be valid only on a case-per-case basis, especially in the identification/separation of photons and electrons. The second study was focused

on the detection of converted photons product in air, and the separation power with respect of the rest of the radiation field detected. Other ionizing radiation produced by photons in the surrounding material has to be taken into account. The GEANT4 simulation of the experiment has shed light on the problem by showing that the bound back-scattered signal can generate an overwhelming contribution that prevents us to distinguish electrons coming from Compton effect in the air. This result is a key to understand the behaviour of Medipix devices installed with considerable amount of neighbouring material.

### Acknowledgements

This work has been done in the framework of the CERN Medipix Collaboration. It has been supported by the Natural Sciences and Engineering Research Council of Canada (NSERC), the Canada Foundation for Innovation (CFI) and the Ministry of Education, Youth and Sports of the Czech Republic under Research Projects MSM 6840770029 and LA08015. C. Teyssier acknowledges the French Ministry of research for doctoral fellowship.

### References

- [1] Medipix Collaboration: <<http://medipix.cern.ch/MEDIPIX>>.
- [2] J. Bouchami, et al., Study of the charge sharing effect in silicon pixel detector by means of heavy ionizing particles interacting with a Medipix2-USB device, Nucl. Instr. and Meth. A (2010), doi:10.1016/j.nima.2010.06.141.
- [3] J. Bouchami, et al., User-extensible implementation of a pattern recognition algorithm for imprints produced by ionizing radiation in a device from the Medipix family, Nucl. Instr. and Meth. A, submitted for publication.
- [4] X. Llopert, R. Ballabriga, M. Campbell, L. Tlustos, W. Wong, Timepix, a 65k programmable readout chip for arrival time, energy and/or photon counting measurement, Nucl. Instr. and Meth. A 581 (2007) 485.
- [5] J. Bouchami, et al., Measurement of pattern recognition efficiency of tracks generated by ionizing radiation in a Medipix2 device, Nucl. Instr. and Meth. A (2010), doi:10.1016/j.nima.2010.06.163.
- [6] M. Campbell, et al., The measurement of spectral characteristics and composition of radiation in ATLAS with MediPix2-USB devices, in: M. Barone et al. (Eds.), Proceedings of the 10th International Conference on Advanced Technology and Particle Physics, Villa Olmo, Como, Italy, October 8–12 2007, World Scientific, Singapore, 2008, p. 346.
- [7] NuDat2: <<http://www.nndc.bnl.gov/nudat2/>>.
- [8] J. Jakubek, Precise energy calibration of pixel detector working in time-over-threshold mode, Nucl. Instr. and Meth. A, (2010), doi: 10.1016/j.nima.2010.06.183.
- [9] H.E. Johns, J.R. Cunningham, The Physics of Radiology, fourth ed., Charles, C. Thomas Publisher, 1983.
- [10] S. Agostinelli, et al., Nucl. Instr. and Meth. A 506 (2003) 250.
- [11] J. Allison, et al., IEEE Trans. Nucl. Sci. NS-53 (2006) 270.